Hindawi Publishing Corporation
Advances in Tribology
Volume 2013, Article ID 657363, 8 pages
http://dx.doi.org/10.1155/2013/657363

Research Article

A Correlative Defect Analyzer Combining Glide Test with Atomic Force Microscope

Jizhong He[1,2]

[1] *Institute of Engineering, College of Engineering, Peking University, Nanjing, Jiangsu 210012, China*
[2] *MicroFocus Technologies, Inc., Wuxi, Jiangsu 214125, China*

Correspondence should be addressed to Jizhong He; jz.he@ufocustech.com

Received 2 January 2013; Accepted 11 February 2013

Academic Editor: Tom Karis

We have developed a novel instrument combining a glide tester with an Atomic Force Microscope (AFM) for hard disk drive (HDD) media defect test and analysis. The sample stays on the same test spindle during both glide test and AFM imaging without losing the relevant coordinates. This enables an in situ evaluation with the high-resolution AFM of the defects detected by the glide test. The ability for the immediate follow-on AFM analysis solves the problem of relocating the defects quickly and accurately in the current workflow. The tool is furnished with other functions such as scribing, optical imaging, and head burnishing. Typical data generated from the tool are shown at the end of the paper. It is further demonstrated that novel experiments can be carried out on the platform by taking advantage of the correlative capabilities of the tool.

1. Introduction

Media defect control has always been a critical part of the HDD manufacturing process. It has a direct effect on the manufacturing product yield which drives the bottom line of business. In the hard disk drive, high media defect level can also cause reliability problems resulting in unforeseen economic losses. Furthermore, defect-free media is an enabler for implementing new HDD technologies. On the other hand, in order to allow high areal density recording necessary for sustained market growth, the head disk spacing in HDD has been pushed down to an extremely small margin [1–3]. As a result, even defects with very small sizes are now becoming serious performance and reliability challenges.

Defect failure analysis (DFA) which analyzes media defects on rejected disks from the production lines plays a central role in the defect process control as it finds the root causes and provides clues for corrective actions. The DFA is done separately from the line test, for example, the glide test. The normal procedure is to send a small portion of the line rejects to the DFA lab where the technicians try to relocate the defects manually, for example, with an optical microscope, before sending them off for examination with an analytical tool such as an AFM. As the criteria for the defects of interest become smaller, manual defect relocation becomes a bigger problem. There are often cases of missed defects when doing DFA or not finding the right ones within the contaminations generated during the handling after the line test, leading to long frustrating days with negative impacts on manufacturing progress.

We have developed a tool which combines glide with AFM. We choose the glide test for its unique sensitivity to only asperities with height, as these are more likely to be in the "killer" defect category in the drive [4, 5]. On the other hand, AFM has been widely used in the medial DFA labs [6, 7]. It provides critical topographic data with the nanometer resolution, perfect for analyzing media defects of the high-density HDD media. AFM has a typical maximum scan range of 100 μm or less. As a result, the defect has to be located right in the middle of the AFM scan range which is oftentimes proven to be difficult to do it manually. This severely restricts the access of the defect analysis with AFM.

The combination of glide with AFM solves a number of problems. It enables an immediate in situ analysis with the AFM after the glide test because the disk sample stays on the same chuck without losing the coordinates. It enables

finding the smaller defects more accurately. The combination also makes the automation possible resulting in orders of magnitude faster throughput for media DFA. We call the tool the Correlative Defect Analyzer (CDA) because multiple tests or analyses are integrated in a single tool to perform on the same correlated defects.

2. Design and Construction

The concept of combining AFM with glide is not new. There was at least one attempt by one of the HDD companies where an AFM module was added to an existing glide tester. No specific technical details are known to the author, but there were reported problems of vibration and weak algorithm, resulting in low AFM image quality and missed defects. (Private communication with relevant engineers familiar with the tool; no commercial product was ever released to the general market.)

The CDA tool described in the paper is designed from the ground up. It consists of four major functional blocks; see Figure 1. A spindle is mounted on a plate secured to a granite base by a pair of high rigid precision linear guides. A high precision ball screw drives the stage in the X direction as the X-stage; see part A of Figure 1. The ball screw provides a stiffness of 15 N/μm, while the guides secure the lateral movement with a stiffness better than 100 N/μm. The high stiffness is necessary to control the spindle vibration at high RPM. The granite is chosen for its unique vibration damping characteristics. The AFM is mounted on a miniature ball screw stage bolted on a vertical granite arch; see part B of Figure 1. A Z-stage is also mounted vertically on the arch. The Z-stage is comprised of a pair of linear guides, a ball screw driving mechanism, and a housing for the optics. The housing also provides an attachment plane for an automatic turret; see part C of Figure 1. The glide head mount is installed on the automatic turret along with optical objectives, a burnish head mount, and a scriber; see part D of Figure 1.

The air bearing spindle has a dual mode capable of both high speed spinning for glide test, the G mode, and high precision positioning for AFM imaging, the A mode (Chinese patent pending, 201110142434.1). In the G mode, the spindle operates with the controller set to run the RPM to a very low jitter level. In the A mode, the controller is switched to turn the spindle as a rotatory stage capable of a resolution of about 3 arc sec. After the desired location is reached, the lower part of the air support is removed so that the spindle body is pushed down by the upper air support and sits securely to the spindle housing; see Figure 2. The solid contact between the spindle shaft and the spindle housing is necessary for achieving low-noise high-resolution AFM imaging.

Care has been taken during the design phase to select the right components with matching material and functional properties in order to achieve the stringent requirements for long-term stability and high positioning repeatability. To verify the performance of the tool, we have designed experiments to measure the positioning repeatability of the stages. Here in this paper, we only show one example measurement on the X-stage. The measurement method on the other stages is similar.

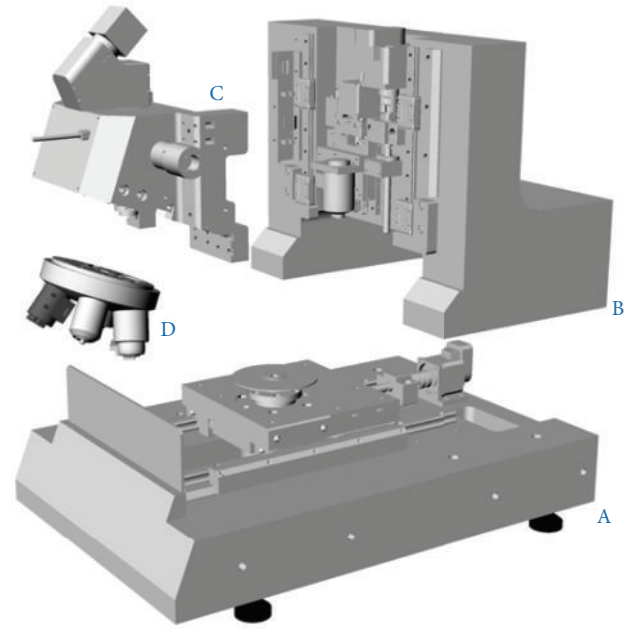

Figure 1: The exploded view of the CDA-101A. Part A, the granite base with the spindle mounted on the X-stage. Part B, the vertical granite arch with the AFM stage and the Z-stage. Part C, the optical housing with CCD camera and automatic turret mount. Part D, the automatic turret with glide, burnish, scriber, and optical objectives. Read the text for further detailed description.

A disk with a micrometer sized defect is clamped on a chuck driven by the X-stage. It serves as the target for measuring the repeatability with the stage repeatedly moved to a predetermined command location. A 50x objective is focused on the disk sample surface and takes the images whenever the disk is moved into the predetermined command position. Images are analyzed automatically by designated software to determine the offset of the target defect to the center. From the offset, the equivalent X-stage position is determined, where the image of the defect will be centered under the microscope.

Statistical data is shown in Figure 3 where the frequency occurrence is plotted against the position of the X-stage with a bin size of 1 μm. At these X-stage positions, the target defect is at the exact center in the microscope view. The scatter of the defect location is attributed primarily to the minute shift in the mechanical stage every time it is moved. The two peaks in the plot indicate the two populations of the stage position. For each population, the stage is found to have very high short term repeatability with a standard deviation of about 50 nm. The reason for the two position population is because that the experiment is carried out at an elevated room temperature first and repeated after overnight cooling at another temperature, resulting in two stable positions at the two temperatures. The overnight temperature swing is about 10 deg Celsius, resulting in a drift of 6 μm. With a characteristic length of 30 cm, this corresponds to 2 ppm/C, a very respectable figure and sufficiently low enough for current applications.

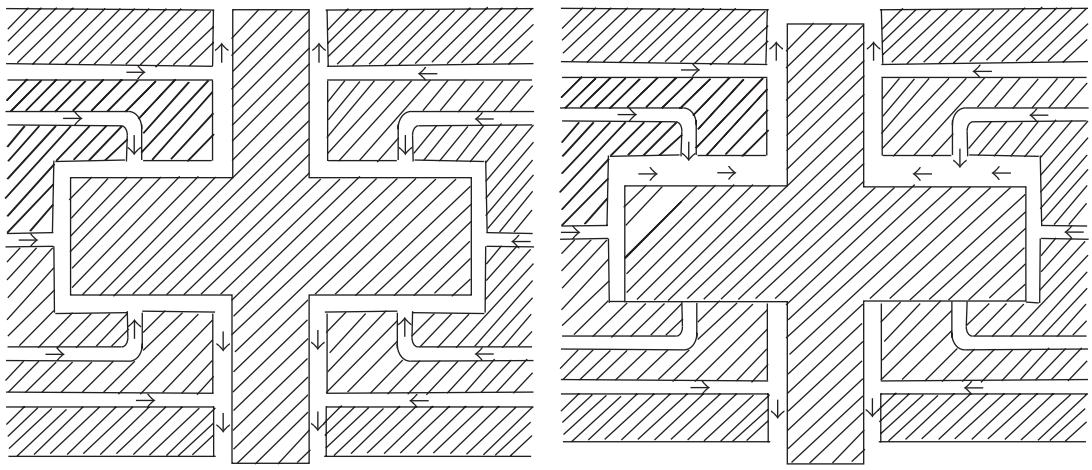

(a) G mode (b) A mode

Figure 2: The dual mode spindle. (a) The G mode. The arrows indicate the flow direction of the air support. In the G mode, the spindle is supported both radially and axially like a conventional air bearing spindle. The spindle is under speed control circuitry to achieve high speed spinning with minimal jitter. (b) The A mode. In the A mode, the spindle is under the positioning control circuitry. It functions as a slow turning rotary table and can be clamped down for imaging when in position. To clamp down the spindle, the bottom axial air support is removed. As the result, the spindle body is pressed against the housing. The working pressure for the air spindle is 5 bars. Note the spindle shown in (b) is already in the clamped position.

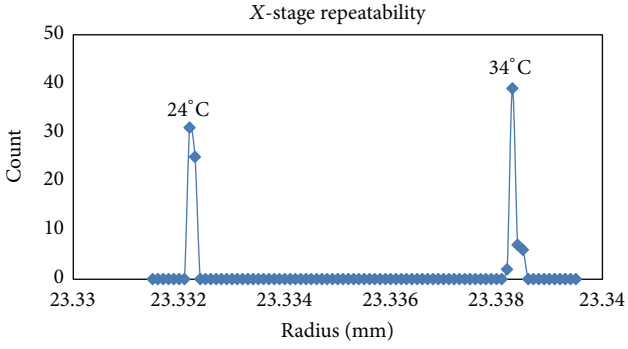

Figure 3: The frequency count plot of the X-stage position, with a bin size of 0.001 mm, that the X-stage must be moved to in order for the target defect to be in the middle of the microscope view. The two peaks correspond to the two highly repeatable positions of 23.332 mm and 23.338 mm due to the two stabilized room temperatures. See text for more detailed description.

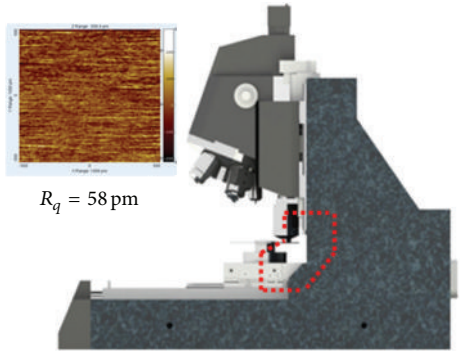

Figure 4: The illustration of the mechanical loop in the AFM. The mechanical loop in sequence consists of the sample, the sample chuck, the stage, the linear guides, the granite base, the granite arch, the approach stage, the scanner body, and the cantilever tip. Test image for noise floor measurement is shown in the insert. The z-scale is ±250 pm. The RMS noise is estimated to be 58 pm.

The AFM scanner is an OEM component. It has a very compact body with a size of a typical microscope objective. The optical interferometry detection scheme has a published noise level of 10 pm. To realize the full potential, we mount the scanner with the approach stage on the massive granite arch to maintain high rigidity. The key is to design the system with the shortest mechanical loop possible; see Figure 4. The short mechanical loop reduces the susceptibility of the scanner to external disturbances. We carry out an effectively still scan (scan range is 1 nm) to measure the mechanical noise floor. Since the tip essentially stays at one spot on the sample, the resulting scan is a measure of the vibration the tip experiences. The data taken with the tool on a homebuilt isolation table without an acoustic enclosure and on the fourth floor of a building shows the RMS noise floor to be about 60 pm. The figure of the noise floor is determined with the commercial application SPIP by using the roughness calculator (SPIP SPM Image Processor application by Image Metrology, Horsholm, Demark; the roughness, Sq, calculation at zero scan range by definition is the direct measure of the system mechanical RMS noise floor); see the insert in Figure 4. The image shows overall random signal fluctuation. The streaking in the image is the result of the low frequency noise showing up as an artifact from the raster scan and has no significance towards the calculation of the roughness.

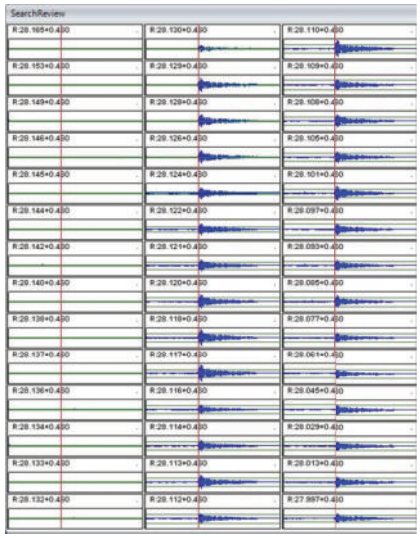

(a) Glide trace panel

1	15	29
2	16	30
3	17	31
4	18	32
5	19	33
6	20	34
7	21	35
8	22	36
9	23	37
10	24	38
11	25	39
12	26	40
13	27	41
14	28	42

(b) Arrangement schematic

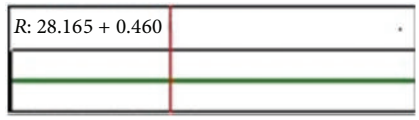

(c) Trace #1

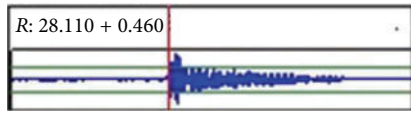

(d) Trace #29

FIGURE 5: Signal analysis panel illustrating the "Glide Edge Finder" algorithm with signal at 42 tracks. The first track with the glide signal is track no. 15 with a radius of 28.130 mm. (a) Glide signal panel showing the signal at each track arranged in descending order of the radius. (b) Schematic of the track arrangement. (c) Signal trace at track no. 1 with the radius equal to 28.165 mm. No signal due to defect is present. (d) Signal trace at track no. 29 with the radius equal to 28.110 mm. Peak signal from defect is present. The starting radius with defect signal defines the edge, 28.130 mm. The value 0.460 mm is the glide head edge offset. The angle is obtained from the averaging of the peak angular position of the data, shown as the red line in (a).

3. Defect Indexing and Unified Coordinate System (UCS)

The width of a typical glide head is about one millimeter. Glide heads with wider sensor area can complete a full surface scan in fewer tracks. This is necessary in order to meet the throughput requirement on the production lines because every disk goes through the glide before shipping. Due to the large sensor width, the uncertainty from the glide test is about a few hundred micrometers in the radial direction and a few millimeters in the track direction. We have developed a "Glide Edge Finder" algorithm that narrows down the location of the defects to within 5 μm. The algorithm moves the glide head track by track in very fine steps in the vicinity of the defect based on results from the prior glide test. It finds the edge of the glide head where the defect first makes contact with the glide head. This method is independent of the shape of the glide air bearing slider. However, the exact shape of a glide head does affect the glide head edge offset. As a result, every new glide head will need to be calibrated for the edge offset when first installed on the tool.

To help explain the process, we show a screen capture of a signal review panel of the CDA software for an actual defect indexing; see Figure 5. The glide signal traces are displayed for each individual tracks. The transition from the tracks with no signal to the ones with signal determines the edge. The angular position is determined by the peak of the signal in relationship to the encoder position of the spindle. For the tracks with the glide signal, the angular positions of the peaks are collected and averaged for statistics. The algorithm has certain logic built-in to handle small defects with marginal signals.

The tool also automatically monitors the glide head position variation, for example, from the time when the glide head is replaced. We have designed an integrated glide head holder which has a set of objective lens group to image the back of the glide head for its exact position. Since it has the optical function of a 5x objective, it is called a glide objective; see Figure 6. The image of the glide head is automatically taken and analyzed by the software for correcting glide head position shift, as much as 100 μm. from head to head. The dimple in the suspension HGA is chosen as the target for position calibration with an estimated uncertainty of about 10 μm. We also integrate the glide channel preamplifier inside the glide objective in order to make the glide head electric connection to the preamp as short as possible in order to achieve maximum SNR.

Since there are multiple tests and sensors correlated in the same tool, there will be multiple position offsets among them to be corrected, for example, between glide and AFM, AFM and optical, AFM and scriber, and so forth. It is one of the goals for the tool to make the offset calibration as transparent

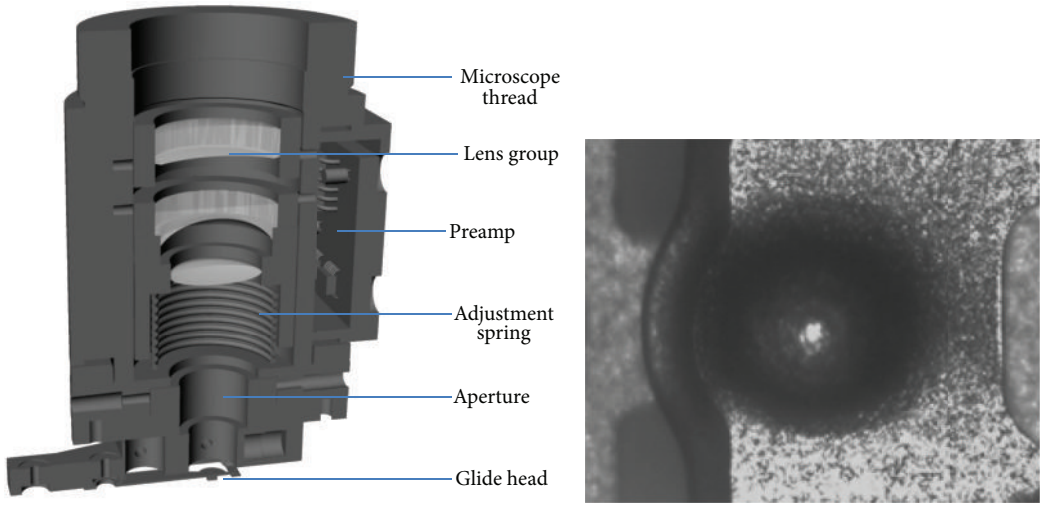

(a) Glide objective (b) Glide head back image

FIGURE 6: Glide objective illustration. (a) shows the internal construction of the glide objective with a 5x lens group enables the imaging on the back of the glide head. An adjustable spring enables the fine focus on the glide head. The preamplifier is integrated to the glide objective to achieve short wire length to the glide sensor. (b) The image of the back of the glide head. In the field of the view, only the center part of the glide head is visible, showing the dimple of the suspension HGA. Glide head position is calibrated against the dimple position.

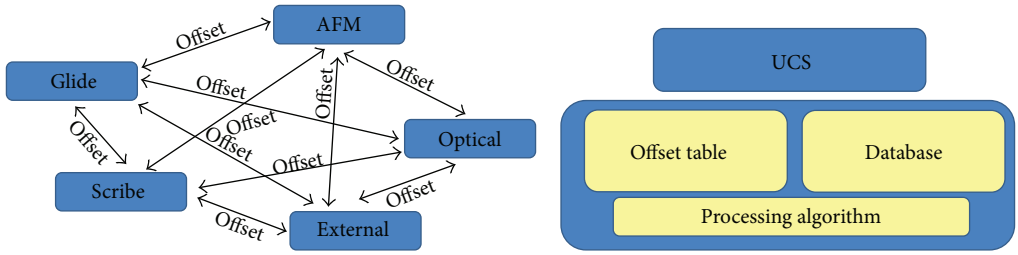

(a) Offset correlation relationship (b) UCS: Unified Coordinate System

FIGURE 7: Schematic drawing showing the relationship and conversion among various coordinate systems. (a) Offset transformations that need to be handled if done individually. (b) Unified Coordinate System created to handle the transformation among the various coordinates with background algorithm and offset table. The parameters are stored in the database and undergo constant update when necessary.

as possible to the users. We have developed a Unified Coordinate System (UCS) to handle the transformation. The UCS processes the offset parameters from an offset table. The initial and current parameters are stored in the database processed by the UCS algorithm.

Within the CDA tool, there are multiple sets of coordinates: the stage or machine, the AFM, the glide, the burnish, the scribe, the optical, as well as the external and the UCS. The stage or machine coordinate system is the special one. The tool relies on the stage coordinate system to position the sample. Because of the existing offsets, there will be different stage coordinates for the same physical spot under different sensors. This creates problems for the user practically and sometimes conceptually. The UCS coordinate system is a defined one. It has a specific defined offset relationship with the various sensor coordinate systems, determined by measuring the actual offsets. Under the UCS system, there is only one set of coordinates to deal with by the user. The UCS can also interface with external coordinator systems of customized formats. The function of the UCS is illustrated in the schematics in Figure 7.

4. Example Test

We use a disk from a defunct vintage HDD teardown to test run the CDA tool. Since we have designed a very easy-to-operate user interface, the procedure to run the tool is very straightforward. The sample is loaded and automatically clamped down by a vacuum disk chuck of the conventional design but with increased suction area to meet the specific requirement of the tool. The vacuum chuck is necessary not only for the easiness of mounting samples, but also for the absence of the center obtrusion. This allows a full radius range of the sample for test and analysis and also prevents the possible collision between the chuck and a sensor close to the ID radius.

Following the procedure outlined in Figure 8, the sample goes through the glide test scan first with the CDA in the

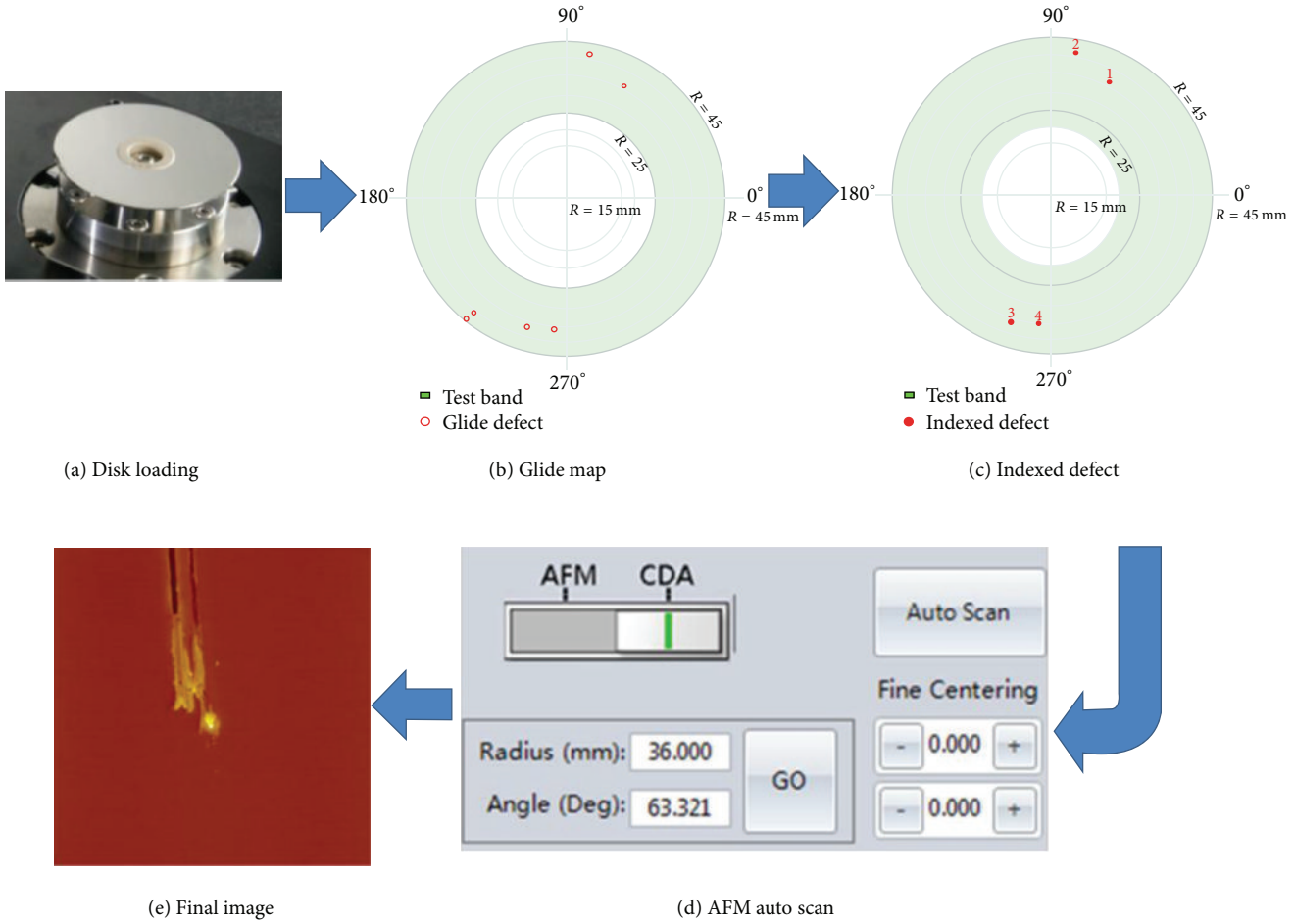

(a) Disk loading (b) Glide map (c) Indexed defect

(e) Final image (d) AFM auto scan

FIGURE 8: Test flow illustration, from sample load to AFM image. (a) Load the disk sample to the chuck. (b) Glide defect mapping from glide test. (c) Map of indexed defect from glide defect search. (d) CDA to AFM switch panel. A simple press of the "Auto Scan" button will start the automatic AFM scan routine. (e) Final AFM image of one of the scanned defects.

G mode. The operator then selects which one, or all, of the defects for AFM imaging. An indexing run follows on the selected defects before the tool is switched to the AFM mode or the A mode. After the indexing run, the selected defects can be relocated with an uncertainty of $\pm 5\,\mu$m. The AFM scan can be carried out either manually or fully automatically. The automated AFM scan procedure includes sample positioning, tip approaching, scanning, tip retracting, and data saving.

The time it takes to complete the whole process depends on a number of factors such as disk form factor, glide head velocity, AFM scanning speed, and the number of scan lines. In general, the time for the initial glide test portion is about 100 sec and about 30 sec additional per defect for the indexing. AFM imaging takes about 130 sec with, for example, 256 lines and 2 Hz scan speed, which produces images with reasonable qualities. So the overall time needed from start to end could be under 10 minutes for one defect, a vast improvement over the traditional DFA involving AFM imaging.

With the precisely known positions, defects can be further analyzed with other available means in the tool such as an optical microscope. For the same defect on the sample disk, the images of the bright field and the dark field optics and the AFM scan are shown together in Figure 9. The defect is visible in the bright field, but the dark field image shows higher contrast and also reveals a long scratch mark originating from the defect. AFM image has much high resolution, showing the defect with a lateral size of about 3 μm and a height of about 30 nm.

Not only the same defect can be analyzed with various sensors, media process specific technology can also be applied to work on the defect correlatively. In our example test, after the initial AFM imaging, a burnish head is used to sweep the defect multiple times. To study the effect of burnishing, the defect is again imaged with the AFM for the second time. The after burnish AFM image is shown in Figure 9(d). The defect retains the same general shape compared with that before the burnish. But the defect height is reduced from 30 nm to 28 nm. We also estimate the apparent volume of the defect before and after with the SPIP software. It turns out the volume number from the software actually increases slightly from 0.080 μm^3 to 0.082 μm^3. We conclude within the experiment error, there is no change in defect volume due to the burnish head sweep. Rather, the contamination on the

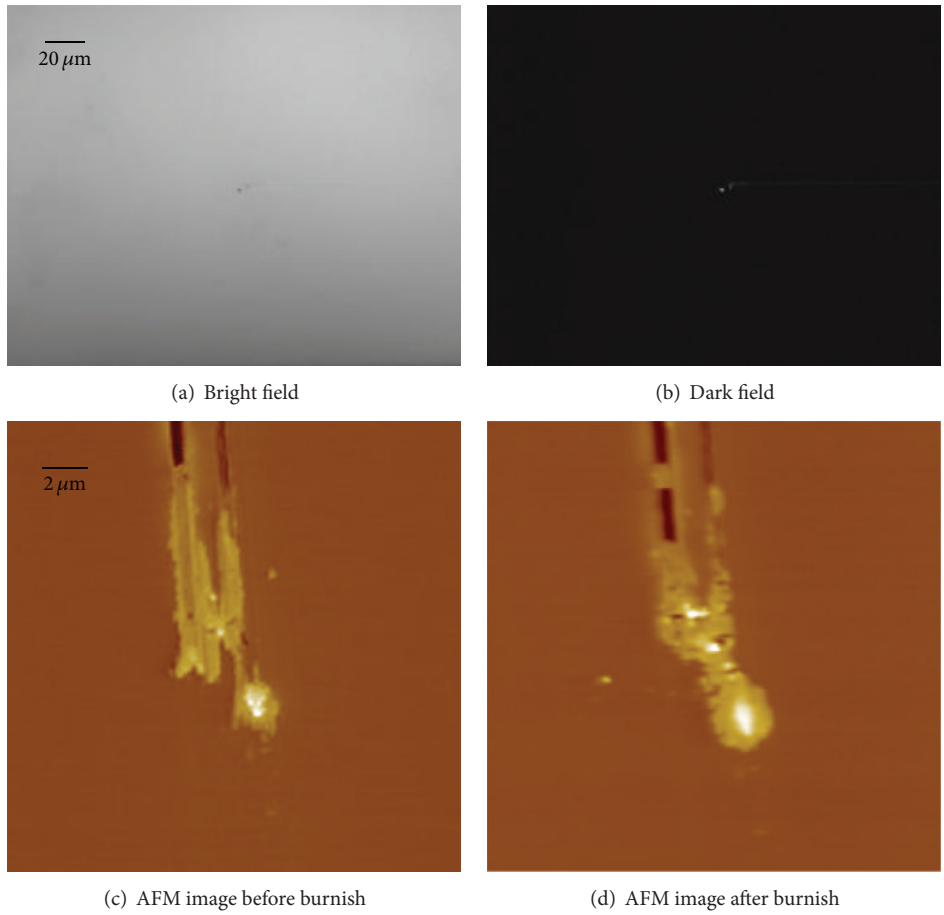

(a) Bright field (b) Dark field

(c) AFM image before burnish (d) AFM image after burnish

Figure 9: Correlated images of a media defect from a teardown disk sample. (a) Bright field image. The defect is very small but can be seen as speck of dark spot in the center of the image. (b) Dark field image. The defect is more visible and a scratch is also revealed against the dark background. (c) AFM images before the burnish sweeps. (d) AFM images after the burnish sweeps.

defect is redistributed. Further more elaborate experiment can be designed and carried out in order to obtain more concrete result on the burnish effect on defects.

5. Conclusion

We have demonstrated a unique tool, combining the glide with the AFM, which can be used to drastically speed up the defect failure analysis process. By performing the AFM analysis in situ, the accuracy of defect relocation and identification is guaranteed. The precision defect indexing algorithm is shown to be robust. High mechanical precision is achieved with the careful selection of components during the design phase. Coupled with the sophisticated software algorithm, a successful correlated defect analysis and a high-resolution low-noise AFM imaging have been demonstrated. With the transparent UCS coordinate system, the users are free from the burden of performing tedious coordinate transformations among the various tests available in the tool. A simple experiment of using the AFM to study the effect of the burnish on the defect shows the advantage of correlative test and analysis. Because of the open frame design and the general layout of the CDA tool, additional processes can be considered for integration into the tool. This will open up new ways of conducting test and analysis by combining various tools in one single unit correlatively.

References

[1] B. Marchon and T. Olson, "Magnetic spacing trends: from LMR to PMR and beyond," *IEEE Transactions on Magnetics*, vol. 45, no. 10, pp. 3608–3611, 2009.

[2] W. Song, A. Ovcharenko, M. Yang, H. Zheng, and F. E. Talke, "Contact between a thermal flying height control slider and a disk asperity," *Microsystem Technologies*, vol. 18, pp. 1549–1557, 2012.

[3] V. Sharma, S. H. Kim, and S. H. Choa, "Head and media design considerations for reducing thermal asperity," *Tribology International*, vol. 34, no. 5, pp. 307–314, 2001.

[4] J. He, G. Sheng, J. Hopkins, and S. Duan, "Head and media instantaneous contact friction measurement and glide test," *IEEE Transactions on Magnetics*, vol. 46, no. 10, pp. 3767–3771, 2010.

[5] H.-L. Leo and G. B. Sinclair, "So how hard does a head hit a disk?" *IEEE Transactions on Magnetics*, vol. 27, pp. 5154–5156, 1991.

[6] Z. W. Zhong and S. H. Gee, "Failure analysis of ultrasonic pitting and carbon voids on magnetic recording disks," *Ceramics International Journal*, vol. 30, pp. 1619–1622, 2004.

[7] J. Windeln, C. Bram, H. L. Eckes et al., "Applied surface analysis in magnetic storage technology," *Applied Surface Science*, vol. 179, no. 1–4, pp. 167–180, 2001.